Available online at www.sciencedirect.com
ScienceDirect
Polymer 47 (2006) 7497–7505
polymer
www.elsevier.com/locate/polymer

The thermal effects on electrospinning of polylactic acid melts

Huajun Zhou [a,b], Thomas B. Green [c], Yong Lak Joo [a,*]

[a] School of Chemical and Biomolecular Engineering, Cornell University, Ithaca, NY 14853, USA
[b] Department of Materials Science and Engineering, Cornell University, Ithaca, NY 14853, USA
[c] United Air Specialists, Inc., Cincinnati, OH 45242, USA

Received 12 June 2006; received in revised form 16 August 2006; accepted 17 August 2006
Available online 7 September 2006

Abstract

We demonstrate that melt electrospinning can be a feasible way to produce sub-micron scale polylactic acid (PLA) fibers in this paper. This solvent-free approach to produce sub-micron scale fibers is more environmentally benign than common solution electrospinning processes, and has a potential to increase the production rate significantly. Our experimental results show that temperatures at the spinneret and in the spinning region are critical to produce sub-micron sized fibers: a high-speed photographic investigation reveals that when spinning temperature is below glass transition temperature, whipping of the jet is suppressed by fast solidification in the spinning region, leading to a larger jet diameter. Both thermal and mechanical degradations of PLA in melt electrospinning can be significant but no change in chemical composition is found. Due to rapid solidification, melt electrospun PLA fibers are mostly amorphous, and the small presence of β crystals is noted in the sub-micron scale PLA fibers by XRD studies. The highly oriented structure of PLA fibers gives rise to cold crystallization at around 95 °C, and the degree of crystallinity of fibers increases with increasing the degree of annealing. Finally, PLA nanofibers have directly been electrospun onto cellulose filter media, and a drastic enhancement in collection efficiency of sub-micron sized dust particles is presented. Melt electrospun PLA nanofiber mats with no residual solvent may serve as better filter media and tissue scaffolds than those obtained from solution electrospinning processes.

Keywords: Polylactic acid; Melt electrospinning; Non-isothermal effect

1. Introduction

Electrostatic fiber spinning or 'electrospinning' is a process for forming fibers with sub-micron scale diameters through the action of electrostatic forces. More than 50 polymers have been successfully spun into fibers through this technique [1]. The collected fibers as non-woven mats have some useful properties such as high surface area to mass ratio, and thus have great potentials in filtration, biomedical, and sensing applications [1–4].

While most previous work on electrospinning has involved polymer solutions [3–7], electrospinning directly from polymer melts can offer several advantages over electrospinning from polymer solution. First of all, dissolution of polymers in organic solvents and their removal/recycling are no longer required. Secondly, a higher throughput can be achieved due to no loss in mass by solvent evaporation. Thirdly, sub-micron scale fibers of polymers which do not have appropriate solvents at room temperature such as polyethylene and polypropylene can be obtained. Multi-component systems such as blends and composites are another example that favors melt electrospinning, because in many cases no common solvent for all of the components may be found. Besides the above advantages, this solvent-free approach also opens the door to theoretical routes to model electrospinning without the complications associated with solvent evaporation.

However, relatively few studies on electrospinning from polymer melts have been reported [8–13]. Some underlying difficulties in melt electrospinning include a high temperature setup, high viscosity and low conductivity of polymer melts.

* Corresponding author. Tel.: +1 607 255 8591; fax: +1 607 255 9166.
E-mail address: ylj2@cornell.edu (Y.L. Joo).

0032-3861/$ - see front matter © 2006 Published by Elsevier Ltd.
doi:10.1016/j.polymer.2006.08.042

In addition, a major drawback of melt electrospinning is that the resulting fibers tend to be relatively thicker than those from solution electrospinning. In the 1980s Larrondo and Manley devised the first melt electrospinning setup [10–12], but the instabilities to cause thinning of the jet via the whipping motion had not been explored. The most recent contribution was made by Lyons and co-workers [8]. They studied the effect of processing parameters on the fiber size of polypropylene and found that the molecular weight is crucial to the final fiber diameter, but key processing parameters such as nozzle size, nozzle temperature and spinning temperature have not been explored.

In our previous structural study on electrospun fibers of PLA from solutions [14], we have reported that molecular structures of electrospun nanofibers are significantly influenced by electrospinning conditions and post-spinning processes, mostly annealing. Highly oriented structures of PLA, which give rise to the formation of a fibrillar β crystal, are observed in solution electrospun fibers. In the current study, we present the effects of processing parameters such as temperature at the nozzle and in the spinning region on melt electrospinning and demonstrate that sub-micron fibers of PLA can also be obtained directly from melt. Thermal properties and structural changes of fibers upon annealing are carefully investigated. In the end, PLA nanofibers are directly electrospun onto filter media, and a drastic enhancement in collection efficiency of sub-micron sized dust particles is presented.

2. Experiments

The experimental setup (Fig. 1) for the current study, as described in detail in our previous work [14], includes basic components such as a digitally controlled syringe pump (PHD2000, Harvard Apparatus), a high voltage supplier (ES30P, Gamma High Voltage Research, Inc.) and a collector as well as some critical components for melt electrospinning such as a heating oven for polymer melt reservoir (T_1), a nozzle heater (T_2), a heated guiding chamber (T_3) and a temperature controllable collector (T_4). Semi-crystalline PLA resins were obtained from Cargill–Dow which have a molecular weight at around 186,000 and polydispersity of 1.76 with major *L* configuration. The glass transition temperature (T_g) of the raw PLA is approximately 55 °C and melting temperature (T_m) is about 165 °C.

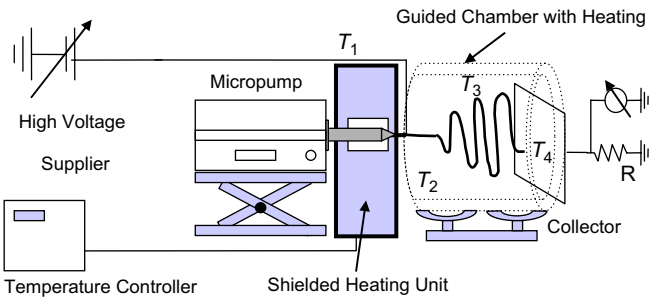

Fig. 1. Schematic diagram of the melt electrospinning setup used in the current study.

In the electrospinning experiments, PLA resins were put in a 5 mL syringe and heated for half an hour in the shielded heating unit at 200 °C. The syringe pump then pushed the PLA melt through a nozzle. The charged melt jet was spun either with or without the heated guiding chamber before being collected on an air-cooled copper collector. Collected non-woven PLA fiber mats were then subjected to characterizations.

Rheological tests were done on a Rheometrics Dynamic Analyzer (RDA II). Processing parameters, such as nozzle temperature, nozzle size, spinning temperature, electrical field and flow rate, were then studied in separate electrospinning experiments. First nozzle temperature (T_2) was varied from 185 °C to 255 °C, while other processing parameters were kept as $T_1 = 200$ °C, $T_3 = T_4 = 25$ °C, $Q = 0.01$ mL/min, $V = 20$ kV, $d = 10$ cm and $D_{nozzle} = 0.16$ mm. Second, the effects of nozzle size were studied using four different inner diameters: 0.84 mm, 0.31 mm, 0.16 mm and 0.13 mm. Other parameters remained the same throughout this study: $T_1 = 200$ °C, $T_2 = 220$ °C, $Q = 0.01$ mL/min, $V = 11$ kV, $d = 10$ cm and $T_3 = T_4 = 25$ °C. Experiments on the effects of spinning temperature were designed by varying T_3 at four different temperatures: 25 °C, 50 °C, 60 °C and 80 °C, keeping $T_1 = 200$ °C, $T_2 = 255$ °C, $T_4 = 25$ °C, $Q = 0.005$ mL/min, $V = 30$ kV, $d = 10$ cm and $D_{nozzle} = 0.16$ mm. Finally, spinning distance and flow rate were adjusted to study the effect of electrical field and flow rate separately by keeping $T_3 = T_4 = 25$ °C.

To probe the motion of the PLA melt jet during electrospinning, a high-speed camera (MotionPro HS-3, Redlake) was utilized. A close-up high-speed (1000–5000 fps) movie of the PLA melt jet near the collector was taken at various spinning temperatures, and selected digitized images were taken to demonstrate the effect of spinning temperature on the whipping motion of the melt electrospun jet.

To study the degradation of PLA molecules during electrospinning, the molecular weight of PLA before and after spinning was measured from the intrinsic viscosity with dilute PLA in chloroform solutions at 25 °C. Morphologies of electrospun fibers were examined by scanning electron microscopy (Leica 440). The thermal properties of melt electrospun fibers were analyzed by differential scanning calorimetry (Seiko, DSC 220C) with a heating rate of 10 °C/min in a nitrogen atmosphere until the temperature reached 200 °C. The structural study was performed through XRD (Scintag, Inc., Theta–Theta Diffractometer). XRD data were collected in the 2θ range of 5–35°, in steps of 0.02° and at a scanning rate of 3 °/min.

The collection efficiency of dust particles in air was measured on a custom-built filtration efficiency tester used officially by United Air Specialists, Inc. Dust particles were counted before and after passing air through the filter media. Air was fed at a rate of 6.9 cfm through each flat-sheet filter and the collection efficiency of dust particles in the size ranging from 0.03 to 5 μm was measured.

3. Results and discussion

3.1. Processing conditions and fiber morphologies

It has been demonstrated that many parameters such as flow rate, voltage, collecting distance, solution viscosity and surface tension have effects on the fiber morphology in solution electrospinning [5–7]. Lyons and co-workers [8] found that in melt electrospinning of polypropylene, the molecular weight and thus the shear and extensional viscosities of the melt play a significant role in obtaining smaller sized fibers. In the present study, we focus on the non-isothermal effects on the fiber morphology by changing the temperature at the nozzle and in the spinning region.

3.1.1. Rheological properties of PLA melt

The melt electrospinning process is strongly influenced by the viscosity of the polymer melt which is typically higher than that of solutions. Therefore, it is important to investigate the rheological behavior of the polymer melt at various temperatures in order to select an appropriate processing temperature. The results of our rheological studies show that the average viscosity of PLA melt is 1 to 2 orders of magnitude higher than that of typical PLA/chloroform solution, and PLA does not exhibit a strong shear thinning over a wide range of shear rates (Fig. 2) [15,16]. The temperature dependence of the shear viscosity for the PLA melt is determined by plotting the logarithm of the zero shear viscosity versus $1/T$ (inset in Fig. 2). The zero shear viscosity is sensitive to temperatures [17] and follows the Arrhenius equation in which activation energy is 83.8 kJ. At the temperature around 240 °C, the zero shear viscosity of the PLA melt is 120 Pa s which is closer to that of some spinnable polymer solutions (117 Pa s for 7.77 wt% poly(*p*-phenylene biphenyl tetracarboxamide acid) in dimethyl acetamide [18]). A wide range of melt temperature (180–255 °C) below the thermal decomposition temperature (330 °C) was applied to investigate its effect on electrospinning. It should be noted that only the nozzle temperature was kept at higher temperature up to 255 °C, while the melt reservoir temperature was always kept at 200 °C since PLA is prone to degradation at a temperature 10 °C above its melting temperature without stabilizers [19–21]. Through this approach, we can minimize the possibility of chemical decomposition during melt electrospinning, while achieving low viscosity at the nozzle. The resident time of the melt in the nozzle is estimated to be less than 0.1 s for a nozzle with ID of 0.16 mm at the typical flow rate of 0.005 mL/min.

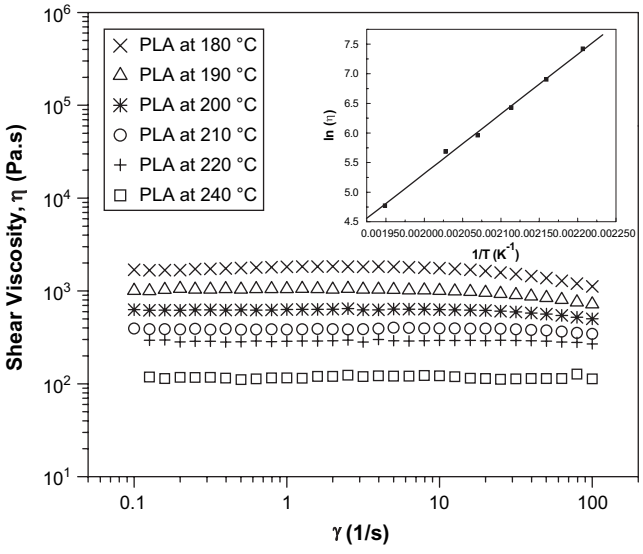

Fig. 2. Shear viscosity and its temperature dependence of neat PLA melt.

3.1.2. Whipping motion of the melt jet

Numerous studies and models [22–25] have confirmed that the whipping motion of the jet in solution electrospinning causes drastic stretching and consequently thins the fiber. However, the presence and characteristics of the whipping motion in melt electrospinning have not been explored. In this section, we report the effect of the spinning temperature on the jet motion and provide an insightful view of the motion of the polymer melt jet during electrospinning. To this end, a high-speed camera was utilized to closely probe the motion of the PLA melt jet in the spinning region. A series of snapshots were taken and (a) the emergence of a limited jet vibration at low spinning temperature ($T_3 = 25$ °C), as we increase the spinning voltage, and (b) the vigorous whipping motion at high spinning temperature ($T_3 = 80$ °C) are shown in Fig. 3. Other experimental conditions including $T_1 = 200$ °C, $T_2 = 255$ °C, $Q = 0.05$ mL/min, $d = 10$ cm, $T_4 = 25$ °C, $D_{\text{nozzle}} = 0.84$ mm are kept constant for both cases.

It should be noted that in Fig. 3(a) the image for $V = 5$ kV was taken at a frame rate of 100 fps, while all others were taken at the frame rate of 1000 fps since the melt jet at $V = 5$ kV moves relatively slow compared to other cases. All the pictures in Fig. 3(b) were taken at the frame rate of 2000 fps due to the strong and fast whipping motion. The dark area on the right-hand side in each image is the collector. The PLA melt jet at $V = 5$ kV has a smooth contour and when the critical voltage 10 kV is reached, the jet starts to vibrate locally near the collector. As a higher voltage is applied, the vibration strengthens and at 20 kV it evolves into a fast spiral movement (whipping). However, the whipping is much weaker and localized compared to that in solution electrospinning [24]. In the case of low spinning temperature, fast solidification of the jet is believed to suppress the whipping motion. When spinning temperature (T_3) is raised to 80 °C, a much stronger whipping motion appears (Fig. 3(b)), which may result in the reduction in fiber diameter, as discussed in the following section. A high spinning temperature above the glass transition temperature can prevent the melt jet from solidifying before reaching the collector. In addition, the strong whipping motion extends the residence time of the jet in the spinning region, enabling the melt jet to go through thinning for a longer period of time. A higher voltage results in even stronger but a more irregular whipping motion as in solution electrospinning. It is also observed that at a low flow rate the whipping motion becomes more vigorous.

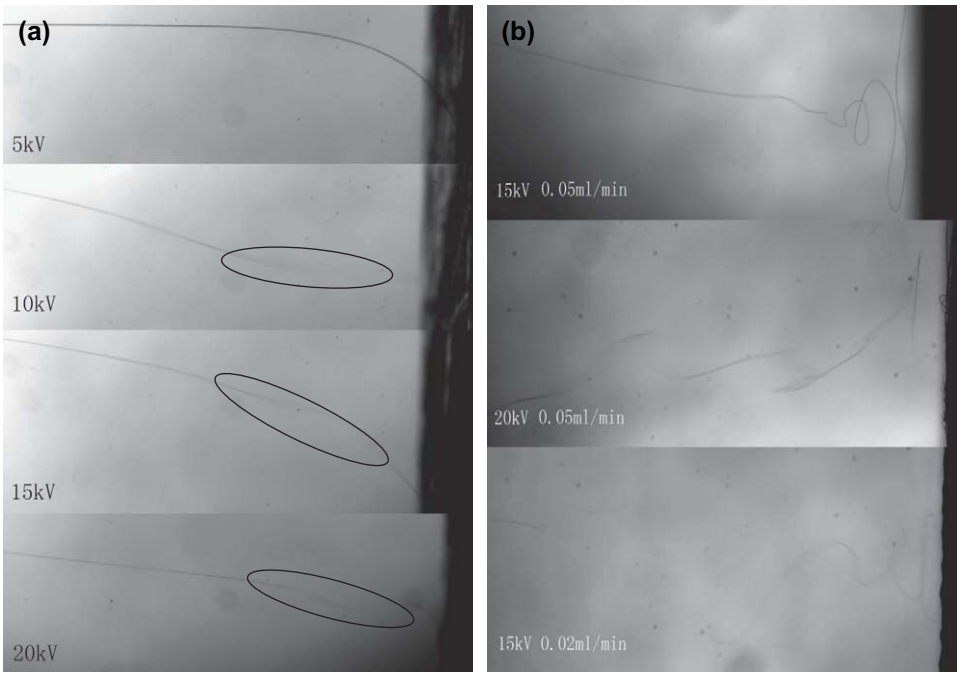

Fig. 3. Effect of voltage on (a) the jet motion at $T_3 = 25$ °C and $Q = 0.05$ mL/min (the limited whipping is pointed out in the oval), and (b) the whipping motion at high spinning temperature ($T_3 = 80$ °C and $Q = 0.05$ mL/min). The last image (in second column) is for small flow rate ($T_3 = 80$ °C and $Q = 0.02$ mL/min).

3.1.3. Effect of processing parameters on fiber diameter

One of the most imperative issues in melt electrospinning is how to obtain sub-micron scale fibers. Hence, we have investigated the effects of various processing parameters on the average fiber diameter. Fig. 4 shows the effects of nozzle temperature on the fiber diameter of melt electrospun PLA fibers. As nozzle temperature increases, both average fiber diameter and standard deviation decrease, and the curve eventually levels out at higher nozzle temperature. According to a recent study on electrically driven viscoelastic fluid flow by Carroll and Joo [26], increasing the fluid viscoelasticity causes a more rapid initial jet thinning. However, farther away from the spinneret, viscoelastic jets are thicker than their Newtonian counterparts due to the higher elongational viscosity. On the other hand, the viscosity of the polymeric liquid mainly influences the initial jet thinning. When spinning and collector temperatures were kept low ($T_3 = T_4 = 25$ °C) such that the whipping motion was substantially suppressed, their results in the stable jet region during electrospinning can be utilized to explain the decrease in fiber diameter with increasing nozzle temperature observed in the current study: the increase in melt temperature decreases the viscoelasticity and thus the final jet gets thinner with increasing nozzle temperature. Nozzle temperatures above 255 °C are not applicable mainly because the elongational viscosity is not high enough to maintain a continuous jet, and as a result droplets of the polymer melt were obtained. A comprehensive modeling of the electrically driven polymer melt jet which incorporates the non-isothermal aspects in melt electrospinning is underway.

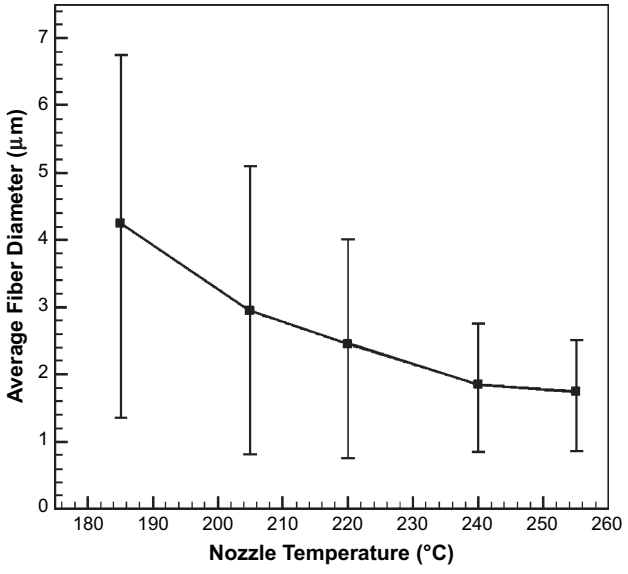

Fig. 4. Effect of nozzle temperature on average fiber diameter (T_3 and T_4 were kept at 25 °C).

Another interesting phenomenon is that a smaller nozzle diameter gives rise to a smaller average fiber diameter, as shown in Fig. 5. Both average fiber diameter and standard deviation linearly decrease as the nozzle size decreases. When the nozzle size becomes smaller than 0.16 mm, the micro-flow controller cannot precisely control the flow rate due to a steep increase in pressure drop. The nozzle size is not discussed often during solution electrospinning but it is a critical parameter to obtain sub-micron sized fibers by melt electrospinning.

The resulting fiber diameter spun at different spinning temperatures is shown in Fig. 6. When spinning temperature is above the glass transition temperature of PLA ($T_3 > 55$ °C), the average fiber size continues to decrease as T_3 increases. It suggests that more deformation is undertaken by the melt

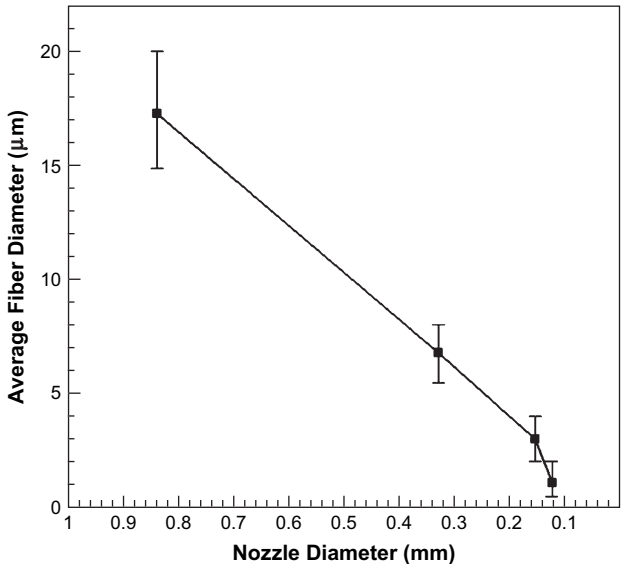

Fig. 5. Effect of nozzle size on average fiber diameter.

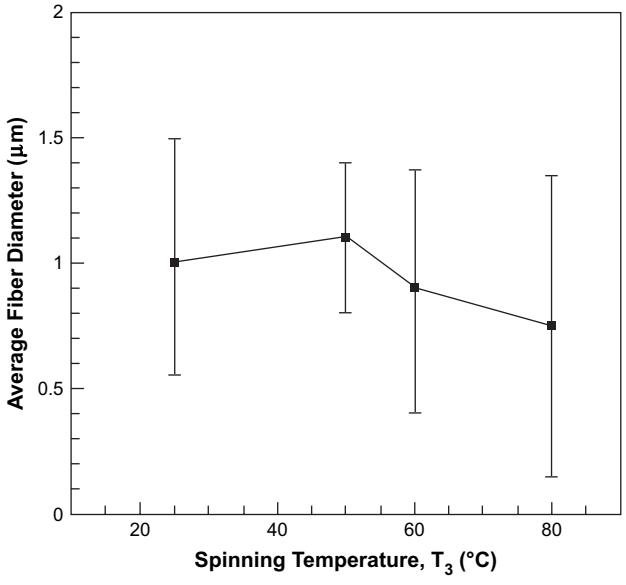

Fig. 6. Effect of spinning temperature (T_3) on average diameter of melt electrospun fibers.

jet at higher spinning temperature, which is clearly caused by the strong whipping motion, as shown in high-speed images. On the other hand, the stronger but more irregular whipping motion at higher temperature presumably results in the greater standard deviation of fiber size distribution.

Other parameters such as flow rate and electrical field were also studied. As electrical field strength increases, the average fiber diameter decreases steadily (Fig. 7). The average diameter of fibers collected at $E = 4$ kV/cm is around 800 nm with a considerable deviation. As for the effect of flow rate, smaller fibers were achieved with decreasing flow rate. The average fiber diameter is 1.7 μm at $Q = 0.01$ mL/min but only 1.2 μm at $Q = 0.005$ mL/min. We note that even at such a small flow rate of $Q = 0.005$ mL/min in melt electrospinning

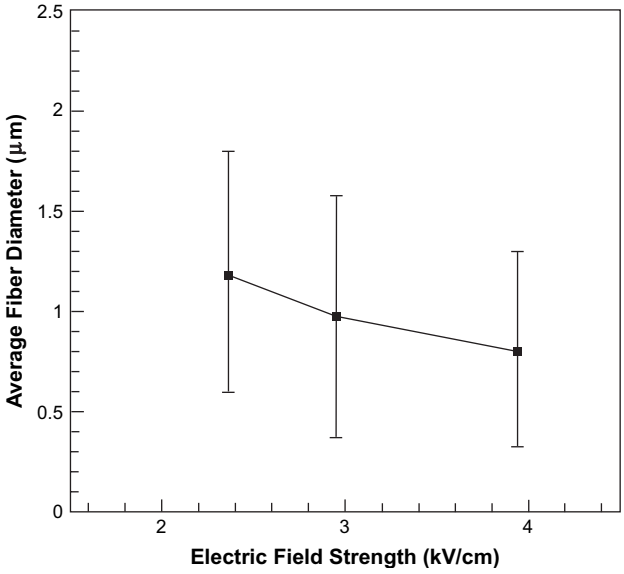

Fig. 7. Effect of electrical field on average diameter of melt electrospun fibers.

the final throughput is 50% higher than that of $Q = 0.02$ mL/min in electrospinning of 12.5 wt% PLA in solution.

The electrospinning parameters that were altered and the results of these experiments are summarized in Table 1.

After combining all the factors considered, PLA melt electrospun fibers with average diameter of 800 nm have successfully been obtained (Fig. 8) under the following conditions: $T_1 = 200$ °C, $T_2 = 255$ °C, $T_3 = 80$ °C, $T_4 = 25$ °C, $Q = 0.01$ mL/min, $V = 20$ kV, $d = 10$ cm and $D_{\text{nozzle}} = 0.16$ mm.

3.2. Degradation in melt electrospinning

Although the thermal decomposition temperature of PLA is around 330 °C, extended exposure of PLA melt to the relatively high temperature in the melt reservoir may still cause thermal degradation. To quantify the degree of degradation before and after melt electrospinning, the intrinsic viscosity $[\eta]$ was measured, and the molecular weight, M_v is calculated by using the following equation [27]:

$$[\eta] = 5.45 \times 10^{-4} M_v^{0.73} \quad (1)$$

It is found that the molecular weight of PLA has changed from the original 186,000 to around 40,000 in the first hour of collection, and after 1 h the rate of degradation slows down for the fibers (Fig. 9). Compared to bulk PLA resins at 200 °C, fibers undergo additional degradation during the spinning process. Two mechanisms of degradation are considered in this process: thermal degradation and mechanical scission. Thermal degradation happens in the melt reservoir and throughout the nozzle. Intramolecular transesterification reaction during heating is the major cause of thermal degradation for PLA below 250 °C [19]. Mechanical scission may take place when the melt is forced through the thin nozzle, and this effect is more prominent when a nozzle with smaller inner diameter (0.16 mm) is used. We also used a nozzle with ID of

Table 1
The summary of electrospinning parameters that were altered and the results of these experiments

Parameter varied	Parameters kept constant	Key observations
Nozzle temperature (T_2) 185 °C → 255 °C	$T_1 = 200$ °C, $T_3 = T_4 = 25$ °C, $Q = 0.01$ mL/min, $E = 2.0$ kV/cm, and $D_{nozzle} = 0.16$ mm	Decrease in fiber diameter
Nozzle diameter (D_{nozzle}) 0.84 mm → 0.13 mm	$T_1 = 200$ °C, $T_2 = 220$ °C, $Q = 0.01$ mL/min, $E = 1.1$ kV/cm, and $T_3 = T_4 = 25$ °C	Decrease in fiber diameter
Spinning temperature (T_3) 25 °C → 80 °C	$T_1 = 200$ °C, $T_2 = 255$ °C, $T_4 = 25$ °C, $Q = 0.005$ mL/min, $E = 3.0$ kV/10 cm, and $D_{nozzle} = 0.16$ mm	Decrease in fiber diameter
Electric field strength (E) 2.4 kV/cm → 4.0 kV/cm	$T_1 = 200$ °C, $T_2 = 220$ °C, $T_3 = T_4 = 25$ °C, $Q = 0.01$ mL/min and $D_{nozzle} = 0.16$ mm	Decrease in fiber diameter
Flow rate (Q) 0.02 mL/min → 0.005 mL/min	$T_1 = 200$ °C, $T_2 = 220$ °C, $T_3 = 80$ °C, $T_4 = 25$ °C, $E = 2.0$ kV/cm, and $D_{nozzle} = 0.16$ mm	Decrease in fiber diameter

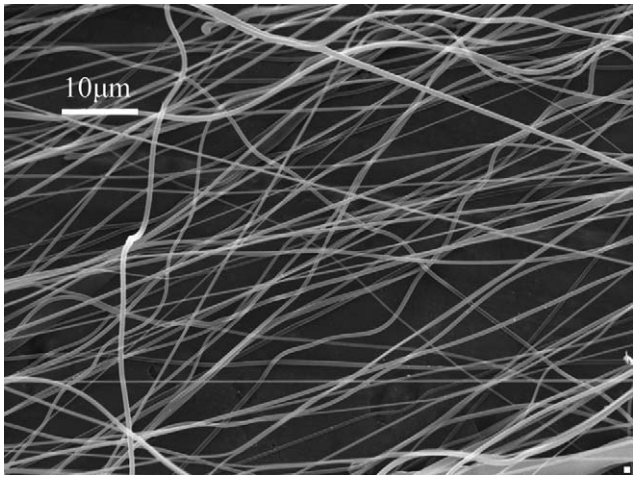

Fig. 8. SEM image of PLA fibers with average fiber diameter of 800 nm directly from its melt.

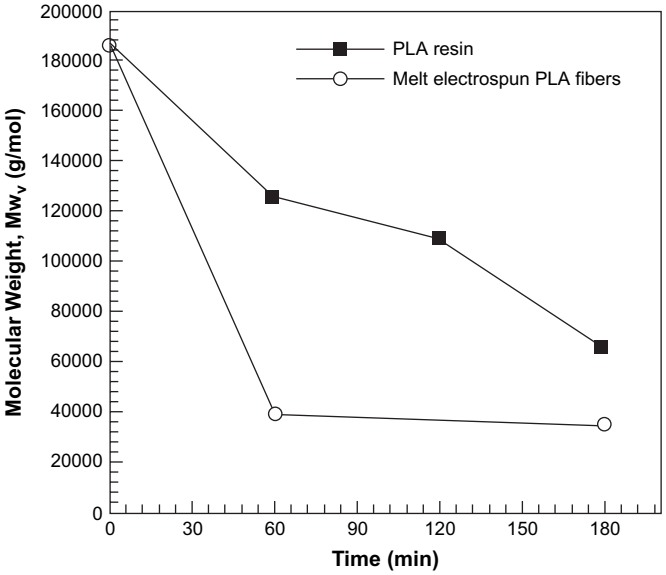

Fig. 9. Thermal degradation of PLA bulk resins and melt electrospun fibers.

0.84 mm to collect fibers and find that fibers collected in the first hour have a molecular weight around 58,000 compared to 40,000 using the 0.16 mm nozzle. The difference is primarily caused by the different extent of mechanical scission. For comparison, the possible degradation during solution electrospinning was also investigated and it was found that no significant degradation occurred.

Although thermal degradation can be minimized by adding a thermal stabilizer [15,20], it can be a useful means to obtain thinner fibers. However, the molecular weight has a close connection with the thermal, structural and mechanical properties. Therefore the discussion that follows is based on the fibers collected during the first 30 min of collecting (and thus with a similar molecular weight).

3.3. Thermal properties of melt electrospun fibers

The jet deformation with fast solidification during electrospinning often results in a meta-stable phase. Since PLA is a slowly crystallizing polymer and its glass transition temperature is above room temperature, fibers were collected at room temperature to study the effect of processing. This is an issue for polypropylene [8,9] since melt electrospun polypropylene fibers cannot maintain the oriented structures at room temperature, and thus a collector cooled below its glass transition temperature by liquid nitrogen was used to keep the aligned structures.

As mentioned in literature [14,28,29], PLA fibers electrospun from solutions usually exhibit a cold crystallization peak through DSC analysis as well as a separation of two peaks near the melting point which gives rise to different crystal structures: α structure with lamellar folded-chain morphology and meta-stable β structure with fibrillar morphology [30]. The presence of cold crystallization in solution electrospun PLA fibers has also been confirmed by the temperature dependent XRD studies in our previous work [14]. Fig. 10 shows the DSC thermograms for two melt electrospun PLA fibers with different average diameters, and they are compared with PLA bulk resin and solution electrospun PLA fibers. Melt electrospun PLA fibers with an average fiber size below 1 μm are produced through the 0.16 mm nozzle, whereas 10 μm-sized fibers are produced through the 0.84 mm nozzle. For all the electrospun fibers from both solutions and melts, a cold crystallization peak at around 95 °C is observed (Fig. 10). Other noticeable characteristics for electrospun fibers are a small melting peak at around 150 °C and a major

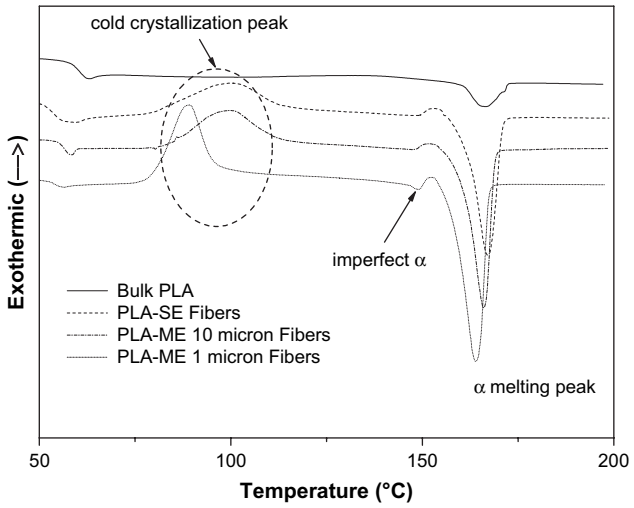

Fig. 10. DSC thermograms for PLA bulk resin and its electrospun fibers.

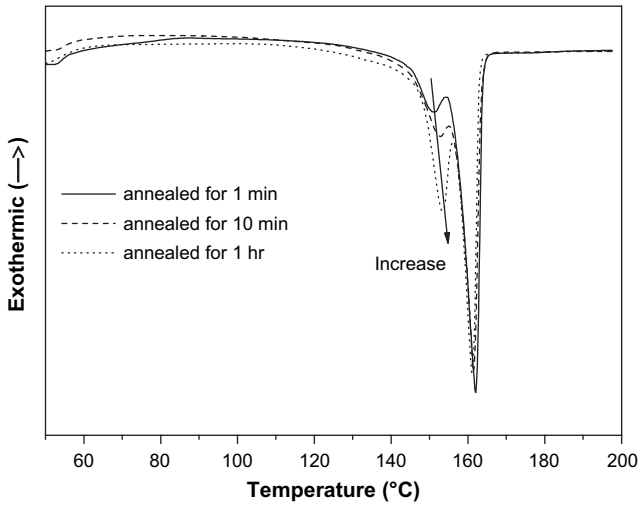

Fig. 11. DSC curves of PLA-ME-1 micron fibers after annealed at 100 °C for various durations.

melting peak at around 165 °C (α crystal). The degree of crystallinity before and after cold crystallization, χ_{bc} (%) and χ_{ac} (%), and temperatures of major peaks from DSC thermograms of various PLA fibers are summarized in Table 2. Crystallinity was calculated based on the following equation:

$$\chi = \frac{\Delta H_f - \Delta H_c}{\Delta H_f^0} \times 100\% \quad (2)$$

where ΔH_f is the heat of fusion, ΔH_c is the heat of cold crystallization and ΔH_f^0 is the heat of fusion for 100% crystalline PLA, 93 J/g [31]. According to Table 2, as-spun sub-micron sized PLA fibers exhibit a small degree of crystallinity which will be verified by XRD studies in the next section, and fibers with different average diameters exhibit different thermal properties. Thick PLA fibers (10 μm) are mostly amorphous, while sub-micron sized PLA fibers exhibit 5.1% crystallinity. After cold crystallization, the total crystallinity of both fibers rises to that of the resin. The lowering of melting temperature of thin fibers is caused possibly by additional mechanical degradation. As we have learned from the degradation study, sub-micron fibers were produced through a smaller 0.16 mm nozzle which can lead to more severe chain scission and thus a lower molecular weight.

To identify the small peak around 150 °C, DSC studies of sub-micron PLA fibers annealed for various durations were carried out (Fig. 11). It is observed that the peak strength around 150 °C gradually increases as the degree of annealing increases, while there is no indication in XRD studies that any β crystals form except α crystals. However, the melting temperature is lower than that of normal α crystals, which is usually identified as imperfect α crystals in PLA [32]. Besides the increase in peak size, we note that the peak shifts toward higher temperature because imperfect α crystals start to convert into perfect α crystals as annealing time increases. Comparing the DSC thermograms of as-spun PLA-ME-1 micron fibers to those of the annealed ones, we also find that upon annealing, the cold crystallization peak almost disappears. In other words, upon annealing, most of the aligned structures have been converted into the α crystal structure. Fibers now exhibit a higher degree of crystallinity compared to its relatively low value before annealing. The XRD study of annealed fibers will also confirm the conversion of aligned structures into the α crystal structure in the next section.

Table 2
Summary of DSC curves for different PLA fibers

Resin/fibers	T_c^* (°C)	T_m^α (°C)	χ_{bc} (%)	χ_{ac} (%)
Bulk PLA	N/A	167.5	46.2	46.2
PLA-SE neat PLA fibers	100.0	167.1	4.8	39.6
PLA-ME-1 micron fibers	88.9	163.9	5.1	49.4
PLA-ME-10 micron fibers	99.8	166.1	0.0	52.6
PLA-ME-1 micron annealed	87.9	163.4	42.6	47.0

3.4. XRD studies and crystal structures

To determine the crystal structures in as-melt spun PLA fibers, X-ray diffraction studies were carried out and the diffraction patterns are shown in Fig. 12. It is observed that

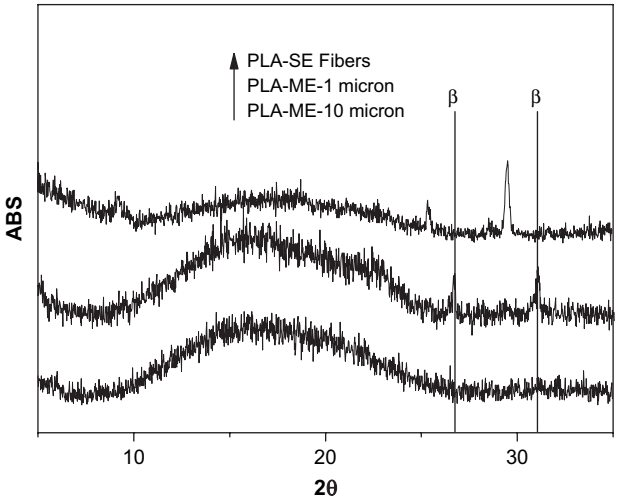

Fig. 12. X-ray diffraction patterns for melt electrospun PLA fibers.

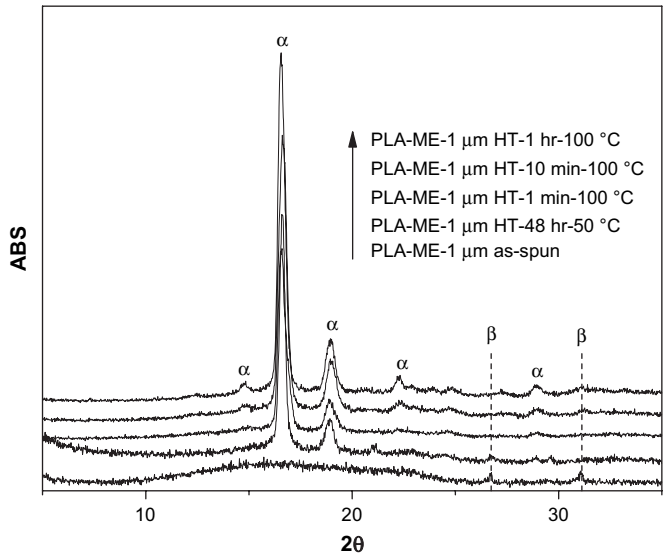

Fig. 13. X-ray diffraction patterns of a series of annealed PLA-ME fibers at different conditions.

melt electrospun PLA fibers of 10 μm scale show a strong amorphous halo, and no distinct crystal peaks are found in the diffraction patterns. On the other hand, sub-micron scale, melt electrospun PLA fibers clearly exhibit two small reflection peaks (near 26° and 31°) ascribed to the β crystals [27]. The formation of β crystals is caused by the different extent of deformation of the polymer molecular chains during the melt electrospinning process [14,30]. The critical factor for the formation of the β crystals is a high degree of deformation (a.k.a. draw ratio in literature [33]). We note that the β crystal peaks of micron sized fibers from PLA melt shift toward higher 2θ values and are also weaker in intensity compared with those of fibers from solution electrospinning probably due to a less degree of whipping (and thus different degree of stretching and deformation of crystal cell constants) in melt electrospinning. Besides these two peaks, we also note that there is a broad shoulder bulging out near 22.8° which can be assigned to the α crystal structure.

It has been reported that the β crystal structure can be converted into the α crystal structure upon annealing. Two annealing tests were carried out: one at 50 °C for 48 h and the other at 100 °C for various annealing durations (Fig. 13). After annealing at 50 °C for 48 h, sub-micron PLA fibers exhibit strong α crystal peaks at 16.7° and 19°, while the β crystal peaks at 26° and 31° almost diminishes. When fibers are annealed at 100 °C even for 1 min, the β crystal structure completely disappears, and strong α crystal peaks form. As the annealing time increases, the strength of all α crystal peaks increases. Hence, we conclude that the small amount of β crystals converts into α crystals upon annealing and after cold crystallization, only α crystals are observed possibly due to this conversion.

3.5. Effect of nanofibers on dust collection efficiency

To study the effect of nanofibers on dust collection efficiency, the PLA melt has been directly electrospun onto the

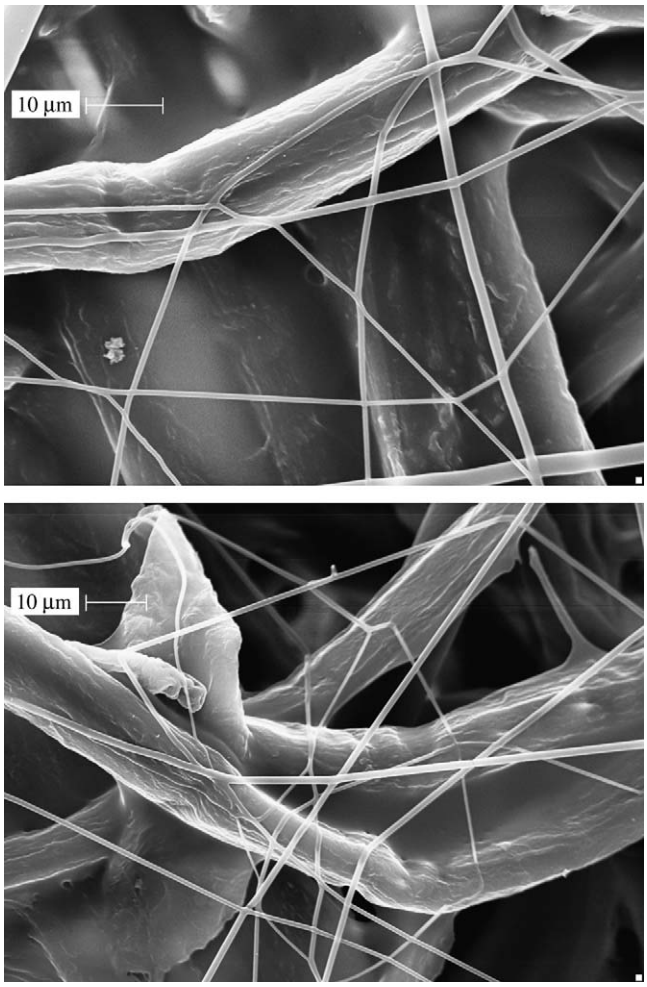

Fig. 14. SEM images of melt electrospun PLA fibers collected on filter media.

cellulose filter media. The SEM images of melt electrospun PLA nanofibers on the filter media are shown in Fig. 14. The average fiber diameter is about 800 nm. It should be noted that a good adhesion between the melt electrospun PLA fibers and the filter media is observed. In fact, some of the electrospun fibers are partially merged to the large cellulose fibers composing the filter media, possibly due to high spinning temperature in the melt electrospinning process.

Finally, the collection efficiency of dust particles in air which was measured using a custom-built filtration efficiency tester is shown in Fig. 15. Four filters were tested, one containing the standard filter media ($12'' \times 12''$), two containing filter media with sub-micron fibers (0.1 g/ft^2 and 0.25 g/ft^2) and an additional filter media covered with 10 μm sized PLA fibers (0.1 g/ft^2) for comparison. It is observed that all the filter media with PLA fibers display a significantly higher collection efficiency of sub-micron sized dust particles with diameters in the range of 0.03–1 μm. However, the gain in the dust collection efficiency for filter media with 10 μm PLA fibers is coupled with an increase in pressure drop (7.5%) compared to the bare filter media; for the same coverage (0.1 g/ft^2) of sub-micron fibers, the increase in the pressure drop due to additional electrospun fibers is below 3.0%. Hence, obtaining

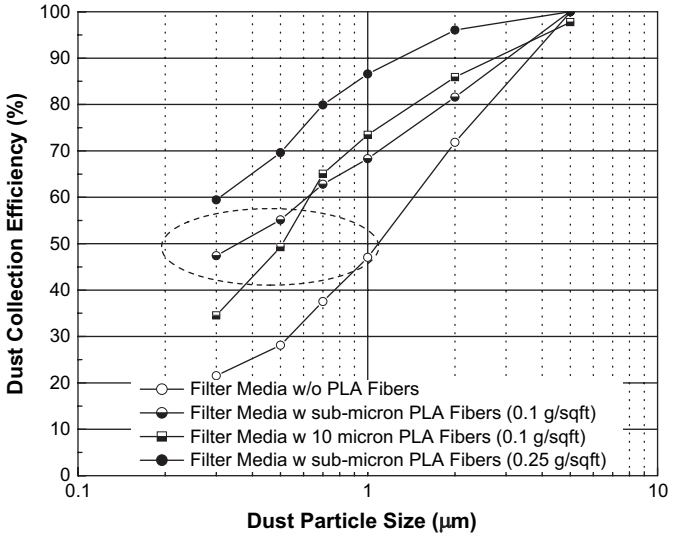

Fig. 15. Dust collection efficiency of flat-sheet filters with and without PLA nanofibers.

the sub-micron scale fibers is crucial to achieve enhanced filtration efficiency without a significant increase in pressure drop. The effect of sub-micron sized fibers on dust collection can be easily illustrated by the higher collection efficiency of dust particles that are smaller than 0.7 μm (refer to the circled region in Fig. 15). Increasing the coverage of sub-micron sized fibers from 0.1 g/ft^2 to 0.25 g/ft^2 drastically increases the collection efficiency, but the percentage increase of pressure drop due to additional coverage of electrospun fibers also rises to 11.1%.

4. Conclusion

PLA is a biodegradable and biocompatible polymer which is being used in many applications including packaging and biomedical fields. It has an ecological significance since it is synthesized from renewable resources. We have demonstrated that sub-micron sized PLA fibers can be directly obtained from melt electrospinning. Compared to solution electrospinning, melt electrospinning has advantages such as a higher throughput and fewer environmental issues. To obtain sub-micron sized fibers, the relationship between processing conditions and fiber morphologies has been investigated and it is found that the temperature at the nozzle and in the spinning region strongly influences the average fiber diameter partially through the thermal and mechanical degradations of PLA. A strong jet whipping motion contributing to reduction in fiber size is observed at high spinning temperature. However, fast solidification caused by low spinning temperature suppresses this whipping motion, and thus results in thicker fibers. The results of our structural studies suggest that melt electrospun PLA fibers can undergo strong deformation during electrospinning and a meta-stable β crystal phase can be formed during the process. The aligned structures in as-spun fibers can be easily transformed into crystal structures by annealing. Finally, PLA sub-micron fibers have been directly electrospun onto filter media, and a drastic enhancement in the collection efficiency of sub-micron sized dust particles has been presented. Melt electrospun PLA sub-micron fiber mats with no residual solvent may serve as better filter media and tissue scaffolds than those from solution electrospinning processes.

Acknowledgements

The authors would like to thank the National Science Foundation for funding this work through a CAREER Award, Grant no. CTS-0448270. This work was supported in part by Clarcor Corporation. We would also like to thank E.I. du Pont de Nemours and Company for funding through a DuPont Young Professor Grant to YLJ.

References

[1] Huang ZM, Zhang YZ, Kotaki M, Ramakrishna S. Compos Sci Technol 2003;63:2223–53.
[2] Groitzsch D, Fahrbach E. US Patent 4,618,524; 1986.
[3] Luu YK, Kim K, Hsiao BS, Chu B, Hadjiargyrou M. J Controlled Release 2003;89:341–53.
[4] Kim K, Yu MK. Biomaterials 2003;24:4977–85.
[5] Zong XH, Kim K. Polymer 2002;43:4403–12.
[6] Jun Z, Hou H, Schaper A, Wendorff JH, Greiner A. e-Polymers 2003;9:1–9.
[7] Doshi J, Reneker DH. J Electrostatics 1995;35(2–3):151–60.
[8] Lyons J, Li C, Ko F. Polymer 2004;45(22):7597–603.
[9] Lyons J. PhD dissertation, Drexel University; 2004.
[10] Larrondo L, Manley SJ. J Polym Sci Polym Phys Ed 1981;19:909–20.
[11] Larrondo L, Manley SJ. J Polym Sci Polym Phys Ed 1981;19:921–32.
[12] Larrondo L, Manley SJ. J Polym Sci Polym Phys Ed 1981;19:933.
[13] Kim JS, Lee DS. Polymer J 2000;32:616–8.
[14] Zhou H, Kim KW, Giannelis EP, Joo YL. In: Reneker DH, Fong H, editors. Polymeric nanofibers. ACS symposium series, vol. 918; 2005.
[15] Lehermeier HJ, Dorgan JR. Polym Eng Sci 2001;41:2172–84.
[16] Cooper-White JJ, Mackay ME. J Polym Sci Part B Polym Phys 1999;37:1803–14.
[17] Dorgan JR, Janzen J, Clayton MP. J Rheol 2005;49:607–19.
[18] Huang C, Chen C, Reneker DH, Lai C, Hou H. Adv Mater 2006;18:668–71.
[19] Wachsen O, Platkowski K, Reichert KH. Polym Degrad Stab 1997;57:87–94.
[20] Södergård A, Näsman JH. Polym Degrad Stab 1994;46:25–30.
[21] Jamshidi K, Hyon SH, Ikada Y. Polymer 1988;29:2229–34.
[22] Shin YM, Hohman MM, Brenner MP, Rutledge GC. Appl Phys Lett 2001;78:1149–51.
[23] Shin YM, Hohman MM, Brenner MP, Rutledge GC. Polymer 2001;42:9955–67.
[24] Fridrikh SV, Yu JH, Brenner MP, Rutledge GC. Phys Rev Lett 2003;90:1445021–4.
[25] Hohman MM, Shin M, Rutledge G, Brenner MP. Phys Fluids 1997;13:2221–36.
[26] Carroll CP, Joo YL. Phys Fluids 2006;18:053102–14.
[27] Schindler A, Harper D. J Polym Sci 1979;17:2593–9.
[28] Zeng J, Chen X, Liang Q, Xu X, Jing X. Macromol Biosci 2004;4:1118–25.
[29] Inai R, Kotaki M, Ramakrishna M. J Polym Sci Part B Polym Phys 2005;43:3205–12.
[30] Hoosteen W, Postema AR, Penning AJ. Macromolecules 1990;23:634–42.
[31] Migliaresi CD, Cohn D, De Lollis A, Fambri L. J Appl Polym Sci 1991;43:83–95.
[32] Yasuniwa M, Tsubakihara H, Sugimoto Y, Nakafuku C. J Polym Sci Part B Polym Phys 2004;42:25–32.
[33] Cicero JA, Dorgan JR. J Polym Environ 2001;9:1–10.